Confined Water Cluster Formation in Water Harvesting by Metal–Organic Frameworks: CAU-10-H versus CAU-10-CH₃

Monique A. van der Veen,* Stefano Canossa, Mohammad Wahiduzzaman, Gwilherm Nenert, Dominik Frohlich, Davide Rega, Helge Reinsch, Leonid Shupletsov, Karen Markey, Dirk E. De Vos, Mischa Bonn, Norbert Stock, Guillaume Maurin, and Ellen H. G. Backus

Several metal–organic frameworks (MOFs) excel in harvesting water from the air or as heat pumps as they show a steep increase in water uptake at 10–30 % relative humidity (RH%). A precise understanding of which structural characteristics govern such behavior is lacking. Herein, CAU-10-H and CAU-10-CH₃ are studied with –H, –CH₃ corresponding to the functions grafted to the organic linker. CAU-10-H shows a steep water uptake ≈18 RH% of interest for water harvesting, yet the subtle replacement of –H by –CH₃ in the organic linker drastically changes the water adsorption behavior to less steep water uptake at much higher humidity values. The materials' structural deformation and water ordering during adsorption with in situ sum-frequency generation, in situ X-ray diffraction, and molecular simulations are unraveled. In CAU-10-H, an energetically favorable water cluster is formed in the hydrophobic pore, tethered via H-bonds to the framework μ–OH groups, while for CAU-10-CH₃, such a favorable cluster cannot form. By relating the findings to the features of water adsorption isotherms of a series of MOFs, it is concluded that favorable water adsorption occurs when sites of intermediate hydrophilicity are present in a hydrophobic structure, and the formation of energetically favorable water clusters is possible.

1. Introduction

Water is arguably the most important molecule on earth. Confined and surface-adsorbed water plays a vital role in many biological, geological, and technological processes. All of the constitutive atoms of water can partake in hydrogen bonds. These hydrogen bonds are relatively strong as an intermolecular force. This has considerable consequences on the adsorption behavior of water into confined spaces, as the confinement effect leads to limitations in the hydrogen networks that can be formed.

Water in micropores (<2 nm) is technologically important. For example, very hydrophilic microporous materials are used as drying agents. Adsorption of water into hydrophilic micropores leads to water uptake at very low relative pressures of water. An example is aluminosilicate type zeolites with low Si/Al ratio where the water dipoles interact strongly with the anionic framework and the countercations.[1] Also in rare

M. A. van der Veen, S. Canossa[+], D. Rega, L. Shupletsov[++]
Catalysis Engineering
Department of Chemical Engineering
TU Delft, Delft 2628, The Netherlands
E-mail: m.a.vanderveen@tudelft.nl
M. Wahiduzzaman, G. Maurin
ICGM, University of Montpellier, CNRS, ENSCM
Montpellier 34293, France

The ORCID identification number(s) for the author(s) of this article can be found under https://doi.org/10.1002/adma.202210050

[+]Present address: Department of Physics, Electron Microscopy for Materials Science, University of Antwerpen, Groenenborgerlaan, Antwerpen 1712020, Belgium
[++]Present address: Chair of Inorganic Chemistry I, Technical University Dresden, Bergstr. 66, 01067 Dresden, Germany

G. Nenert
Malvern Panalytical B. V.
Lelyweg 1, Almelo 7602EA, The Netherlands
D. Frohlich
Fraunhofer ISE
Heidenhofstr 2, 79110 Freiburg, Germany
H. Reinsch, N. Stock
Institut für Anorganische Chemie
Christian-Albrechts-Universität zu Kiel
24118 Kiel, Germany
K. Markey, D. E. De Vos
Centre for Membrane Separations
Adsorption
Catalysis and Spectroscopy for Sustainable Solutions (cMACS)
KU Leuven
Celestijnenlaan 200F, Leuven 3001, Belgium
M. Bonn
Max-Planck Institute for Polymer Research
Achermannweg 10, 55128 Mainz, Germany
E. H. G. Backus
University of Vienna
Faculty of Chemistry
Institute of Physical Chemistry
Wahringerstrasse 42, Vienna 1090, Austria

cases, metal–organic frameworks (MOFs) show strongly hydrophilic character leading to a type-I water adsorption isotherm. An example is CAU-6 due to a large amount of protic functional groups and counterions.[2] In contrast, in hydrophobic microporous zeolites or activated carbons, water adsorption does not occur until very high relative pressures of water. Adsorption branches of the water adsorption isotherm of porous carbons with scarce functional groups show no appreciable water adsorption at room temperature for $p/p_0 < 0.3$, followed by steep uptake between 0.3 and 1 p/p_0.[1] The value of p/p_0 at which this relatively sudden pore filling occurs depends on the pore size, and the more monomodal the pore distribution is, the steeper the increase in the water adsorption isotherm is.[3] Overall, type-V adsorption isotherms ensue, indicative of the formation of an extended hydrogen-bonded network between the adsorbed molecules.[3–5] The shape of type-V isotherms is related to much stronger interactions amongst the adsorbed molecules themselves than between the adsorbate and adsorbent. Also, hydrophobic (all-silica) zeolites[6] and hydrophobic metal–organic frameworks (e.g., water is only exposed to aromatic pore walls without hydrophilic functional groups)[7] show type-V isotherms with steep water uptake only at high p/p_0. Many materials display a water isotherm with intermediate behavior, characterized by gradual water adsorption over a wide range of relative pressures, starting already at low p/p_0. Examples are activated carbons with functional groups[3] and quite some metal–organic frameworks that contain hydrophilic groups.[8]

Intriguingly within the group of microporous materials that would be categorized as of medium hydrophilicity, some materials show a very steep water step in the water adsorption isotherm at relatively low vapor pressure. If this step in the uptake is located between ≈ 0.1 and 0.3 p/p_0, the water adsorption process can be valorized in heat pumps/chillers.[9,10] This particular sorption behavior can also be exploited to harvest water in the desert.[11–14] The shape is more akin to the hydrophobic type-V water adsorption isotherms, except the step occurs at a much lower p/p_0. Yet, the examples of microporous solids that exhibit this unusual intermediate water adsorption behavior important for technological applications are limited.

There are only a few nanoporous materials that show a single steep uptake in the indicated favorable pressure range (between 0.1 and 0.3 p/p_0) with none to very little adsorption at very low p/p_0 values. Among traditional microporous materials, only AlPO-5 stands out. This is a zeotype material with AFI topology with 1D channels. It shows favorable medium hydrophilicity due to its repetitive –Al–O–P– motif, especially when partially iron-exchanged,[15] due to high electrostatic attraction force for water, while not being an H-bond donor. The combination with a 12-membered ring pore geometry commensurate with the adsorbed double water helix leads to a steep water adsorption isotherm in the favorable pressure range.[16] Similarly, the related aluminophosphate VPI-5 has a 1D 18-membered ring pore geometry, commensurate with the adsorbed triple water helix.[17] The steep step in the water adsorption isotherm here occurs already at ≈0.07 p/p_0.[18] Among newer types of materials, a handful of metal–organic frameworks also show these favorable water adsorption isotherms. The advantage of MOFs is that much higher adsorption capacities can be reached with respect to zeolites (up to 0.3 g g^{-1} for zeolites vs 2.0 g g^{-1} for MOFs).[9,19,20]

The structures of the MOFs are nevertheless very different from that of AlPO-5. A tight balance between hydrophilicity and hydrophobicity must be struck to have a favorable water adsorption isotherm. For example, MOFs with coordinatively unsaturated sites are less useful, as water adsorption already starts at very low water vapor pressures owing to the strong affinity of these metal sites to water.[21] MOFs with pores above a critical diameter (2 nm at room temperature) show undesirable, irreversible, and discontinuous water adsorption due to capillary condensation.[8,22] Moreover, MOFs that lack hydrophilic sites and very narrow pore windows, like ZIF-8, behave like superhydrophobic materials.[23] The key to achieving favorable water isotherms seems to be an interplay of moderately hydrophilic (e.g., framework hydroxyl groups) and hydrophobic sites (e.g., phenylene groups) within mere nanometres. But even among the MOFs that display this alternation, only a handful show none to very little adsorption at very low p/p_0 values, followed by a very sharp step change in the desired 0.1–0.3 p/p_0 range, namely MOF-801(Zr),[24] Al-fumarate,[25] MOF-841(Zr),[24] MOF-333(Al),[26] CAU-23(Al),[27] Co-CUK-1,[28] Ni-CUK-1[28] and CAU-10-H(Al).[29] All these materials show a combination of hydrophobic conjugated aromatic moieties combined with hydroxyl-containing inorganic units. Very insightfully, Yaghi et al.[26] recently showed for MOF-303, a structure containing framework hydroxyl groups, that replaced its hydrophilic linker 1-H-pyrazole-3,5-dicarboxylate with much more hydrophobic 2,4-furandicarboxylate—leading to the isostructural MOF-333—enables water adsorption at very low relative humidity values to be suppressed, and induces a much steeper step in the water adsorption isotherm, located at 0.22 p/p_0. Also, the promising water adsorbent CAU-10-H has recently been compared with its functionalized forms incorporating hydrophilic groups, i.e., CAU-10-NO$_2$ and CAU-10-NH$_2$.[30] These studies reiterate that the combination of hydrophobic conjugated aromatic moieties with a few more hydrophilic sites, e.g. hydroxyls contained in the inorganic units, is key to achieving good water harvesting properties. Yet, there is also a wealth of MOFs that consist of such units, but nonetheless do not show the desired water adsorption behavior. This paper aims to answer the question of what structural features must be present in a MOF in order to exhibit favorable water adsorption behavior.

Here, we especially contrast CAU-10-H, [Al(OH)(C$_8$H$_4$O$_4$)], and CAU-10-CH$_3$, [Al(OH)(C$_9$H$_6$O$_4$)]. Their structures consist of infinite helical chains of cis-connected, corner-sharing AlO$_6$ octahedra, which are connected into a 3-D framework by isophthalate (CAU-10-H) or 5-methylisophthalate (CAU-10-CH$_3$) anions. Both frameworks are isostructural and have the same amount of hydrophilic (Al–OH) and hydrophobic features (isophthalate with or without −CH$_3$ functionalization) in their unit cell. Yet, their water adsorption behavior is distinctly different. While CAU-10-H shows an impressive step-change within the ideal relative humidity range (0.18 p/p_0 at ambient temperature), the H$_2$O adsorption isotherm of CAU-10-CH$_3$ shows a much more gradual increase, where half of the saturation capacity is only reached at 0.45 p/p_0 (see **Figure 1**). The CAU-10-H structure is also of particular relevance application-wise, as it has been shown to retain its capacity after 20 000 drying/wetting cycles.[31,32]

Here, we reveal via the combination of single-crystal X-ray diffraction (XRD) and force-field Monte Carlo/quantum calculations that the origin for this difference is the formation of an
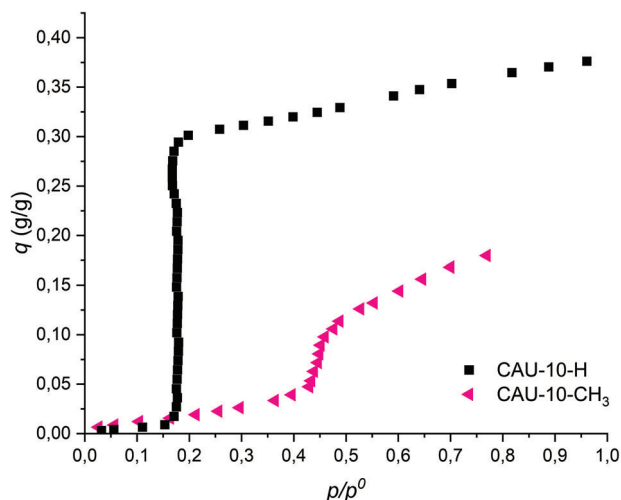
2210050 (2 of 13)

Figure 1. Water adsorption isotherms of activated CAU-10-H, CAU-10-CH$_3$. Reproduced with permission.[29] Copyright 2013, American Society of Chemistry.

energetically far more favorable water cluster in CAU-10-H versus CAU-10-CH$_3$. We unravel further intricacies of the phase transitions accompanying water adsorption via second-harmonic generation (SHG), sum-frequency generation (SFG), and XRD at varying relative humidity values. Furthermore, we provide a broader perspective on what determines favorable water adsorption in MOFs by relating our conclusions to the water adsorption isotherms of a series of MOFs.

2. Results and Discussion

CAU-10-X (X = −H, −CH$_3$) was synthesized according to the procedures of the original publication (see Section 1, Supporting Information for details).[29] CAU-10-H shows a phase transition from a centrosymmetric to a non-centrosymmetric structure upon water adsorption,[31] which can be detected via second-harmonic generation (SHG) or frequency doubling of light, as this is only allowed for non-centrosymmetrically organized matter. The centrosymmetric and non-centrosymmetric structure of CAU-10-H is shown in Figure S2.2.5 (Supporting Information). In fact, here we find that both CAU-10-H and CAU-10-CH$_3$ undergo a such phase transition, as at high humidity values when both materials are hydrated, clear SHG light intensity is present in the SHG-images (**Figure 2**a, top), while at low humidity values, when both materials are dehydrated, no SHG signal is detected (Figure 2a, bottom). Thus, the MOF host/water guest interaction is sufficiently strong to induce a phase transition.

Sum-frequency generation (SFG), like SHG, occurs only for non-centrosymmetrically organized matter. If one of the two frequencies of light that are summed, belongs to the mid-IR range, then vibrational spectra specifically of non-centrosymmetric structures can be obtained. In Figure 2b,c, the SFG spectra demonstrate that for each compound, peaks are only visible for the water-filled structures at elevated relative humidity values, again confirming the centrosymmetric to non-centrosymmetric phase transition upon water adsorption. In addition to the vibrational peaks of the MOFs themselves (≈ 3650 cm^{-1} −OH stretch-

ing vibration of μ−OH, ≈ 3050 cm^1 aromatic −CH stretching vibration), also the broad peak of the −OH stretching vibrations of the adsorbed H$_2$O (≈ 3100–3500 cm^{-1}) is SFG-active at high relative humidity. This means that also the adsorbed water is organized in a non-centrosymmetric arrangement. Both the MOF structures and water clusters are impacted structurally by their interaction. Moreover, we find via humidity-dependent SHG and SFG measurements, for CAU-10-OH and CAU-10-NO$_2$ that the same transition of a centrosymmetric to non-centrosymmetric takes place upon hydration with non-centrosymmetrically organized water in the pores (Figures S4.3.1, S4.3.2, and S4.4.1 in the Supporting Information). Additionally, we report for the first time a Rietveld refined structure for guest-free CAU-10-NO$_2$ and CAU-10-OH (Section 2.1, Supporting Information).

To understand the structural changes upon water adsorption in CAU-10-H and CAU-10-CH$_3$, both powder XRD and SFG experiments have been performed under varying relative humidity. To measure the ν(CH) and ν(OH) vibrations simultaneously, a femtosecond pulsed mid-IR envelope, of 700 cm^{-1} width, needs to be used. This could only be obtained by maintaining the Optical Parametric Amplifier (OPA) in a metastable state. As such, during the measurements at varying relative humidity, small drifts of the mid-IR envelope could not be avoided. Therefore, for both CAU-10-H and CAU-10-CH$_3$, three independent data series were obtained, all reported in the (Sections 4.2 and 4.5, Supporting Information). The trends discussed here, are only those that are consistent with all datasets.

The resulting SFG peak normalized intensities corresponding to the aromatic ν(CH) and ν(OH) stretching vibrations of CAU-10-H (see Section 4.5, Supporting Information, for explanation of the data treatment), are shown in **Figure 3**a and Figure S4.5.1 in the Supporting Information as a function of relative humidity. As shown before, for the dehydrated phase (RH% < 18) there is no SFG activity. The SFG intensity sharply increases ≈ 18 RH%, above which both $I_{SFG}(\nu(\text{CH}))$ and $I_{SFG}(\nu(\text{OH}))$ remain largely constant. This step change in the SFG spectrum is indicative of a first-order phase transition of the structure.

For CAU-10-H, the powder X-ray diffraction (PXRD) data collected as a function of their relative humidity during adsorption and desorption are shown in Figure S5 in the Supporting Information. At low relative humidity values, before the abrupt adsorption of water, a single X-ray diffraction pattern is found; at higher relative humidity values also a single, but different X-ray diffraction pattern is observed. Hence, we show in Figure 3b only the narrow range of relative humidity values in which the phase transition takes place. The phase transition takes place in a very narrow range from 15 to 16.5 RH%, indicated by the curly brackets in Figure 3b. The PXRD patterns in this transitional region, are in fact a superposition of the PXRD patterns of the water-filled and empty H-CAU-10 structures, indicating an abrupt change in structure. Likely, the occurrence of both PXRD patterns at the same time is due to kinetic effects. Also, these data are indicative of a first-order phase transition. Note that while at room temperature, the phase transition takes place at 18 RH% (4 g m^{-3} water vapor), in the XRD measurements the phase transition takes place at a lower relative humidity value of 16% due to the higher temperature of 40 °C (16 RH% = 8 g.m^{-3} water vapor).

For CAU-10-CH$_3$, the SFG spectra were also obtained under varying relative humidity values. The resulting peak intensities

**ADVANCED
SCIENCE NEWS**

www.advancedsciencenews.com

**ADVANCED
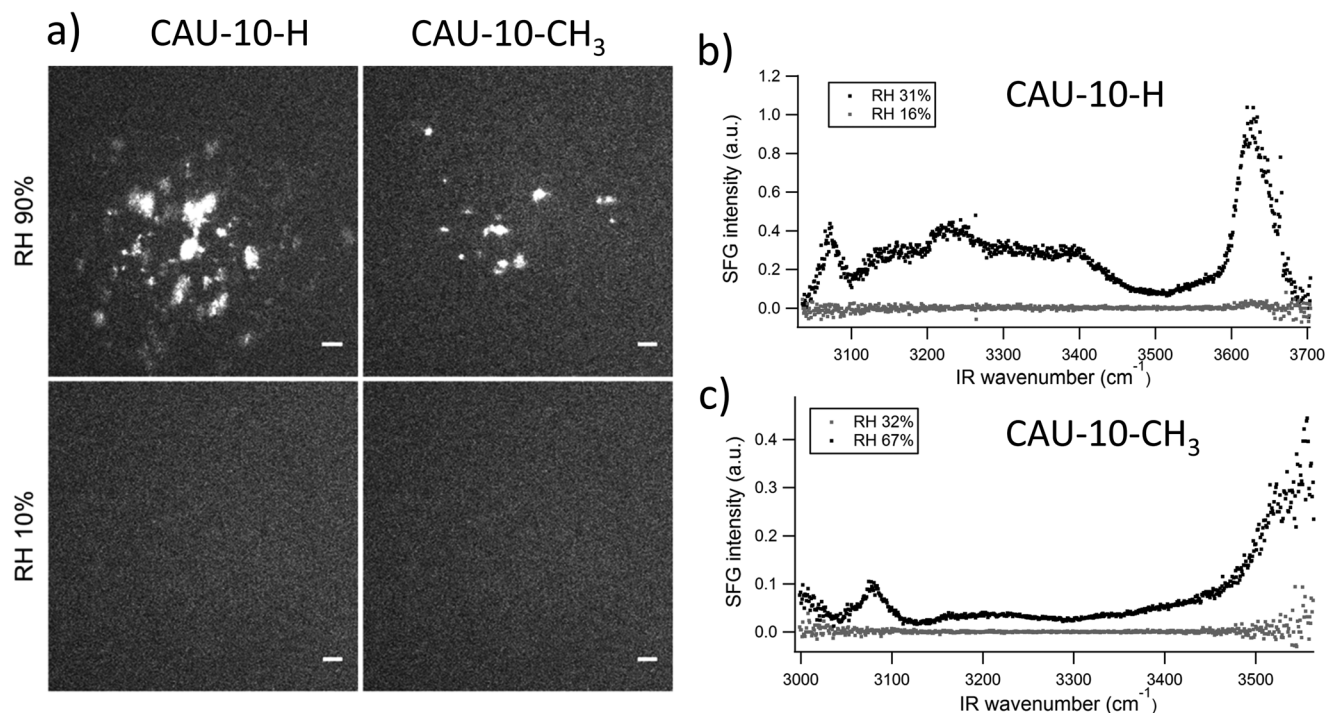MATERIALS**

www.advmat.de

Figure 2. a) SHG-images using 800 nm incident light, and detecting 400 nm light in transmission of CAU-10-H (left) and CAU-10-CH₃ (right) powders at room temperature at 90% relative humidity (top) and at 10 RH% (bottom). The scale bars indicate a length of 20 μm. b,c) SFG spectra at room temperature of CAU-10-H at 16 and 31 RH% (b) and CAU-10-CH₃ at 32 and 67 RH% (c).

of the aromatic ν(–CH) and ν(–OH) peaks as a function of relative humidity for CAU-10-CH₃ are presented in **Figure 4**a and Figure S4.5.2 (Supporting Information), and for the aliphatic and aromatic ν(–CH) in Figure S4.5.3 (Supporting Information). We see a more gradual increase in SFG intensity with relative humidity compared to CAU-10-H. The PXRD data at varying relative humidity for CAU-10-CH₃ (Figure 4b) show a very different picture than those for CAU-10-H. Between 30 and 60 RH% several diffraction peaks change their position and relative intensities, and at the same time, some new peaks appear. These changes are indicated by the rectangles that serve as guides-to-the-eye in Figure 4b. The humidity-dependent SFG and XRD results indicate a gradual, hence higher-order phase transition. Interestingly, in the SFG data in Figure 4a and Figure S4.5.2 (Supporting Information), we see at low relative humidity values (up to 45 RH%) that an SFG signal corresponding to the ν(–OH) vibration already appears, while the SFG-intensity corresponding to ν(–CH) vibration is not observed (Figure S4.5.3, Supporting Information). This could mean that at low adsorbed water content, the framework –OH is distorted relatively more into a non-centrosymmetric arrangement than the –CH vibration, at higher water content, this difference fades out. For an unfunctionalized metal–organic framework without unsaturated coordination sites, the M–OH sites are those where one indeed expects the first water molecules to adsorb via H-bonds.[28,33] At higher adsorbed water content, also the –CH bonds organize into a non-centrosymmetric arrangement, meaning that the aromatic hydrophobic cavities are most deformed at high filling levels.

The precise structure of the non-centrosymmetrically organized water molecules in CAU-10-H is deduced from single-

crystal XRD data. Following the method developed by some of the authors,[34] via the addition of an oxalic acid modulator, ≈12 × 8 × 8 micrometer-sized crystals of CAU-10-H were grown on which we performed single-crystal XRD at 100 K with bright synchrotron radiation. The hydrated compound crystallizes in space group $I4_1md$ rather than $I4_1$ as previously reported by some of us[29] (see Section 2.2, Supporting Information). In Section 3, Supporting Information, a detailed tabulation and discussion of all the different space groups reported in literature for CAU-10-X can be found, as well as those based on the refinements in this work (vide infra).

Well-defined water clusters are detected, via distinct positions of the O-atoms, in the pores. As shown in Figure S2.2.4 in the Supporting Information, from Rietveld refinement against PXRD patterns, similar positions of the water O-atoms are found at room temperature both for products from an oxalate-modulated synthesis as well as from the original synthesis.[29] There is thus an agreement between the single crystal X-ray diffraction data at 100 K and the powder X-ray diffraction data at room temperature.

The O-positions refined from single crystal XRD are shown schematically in **Figure 5**a and consist of a double pentamer, of which one square is tethered via four water molecules that are hydrogen bonded to the –OH groups of the AlO₆-chains (Figure 5d). The distance of the tethering water oxygen atom to the proton of the framework –OH is with 2.03 Å (and with 2.818(8) Å between the oxygen atoms) in the range of characteristic H-bonding distance (**Table 1**). The O3 atoms of the water pentamer are also within hydrogen bonding distance of framework carboxylate oxygen atoms (3.06 Å). The two water molecules tethered to the top
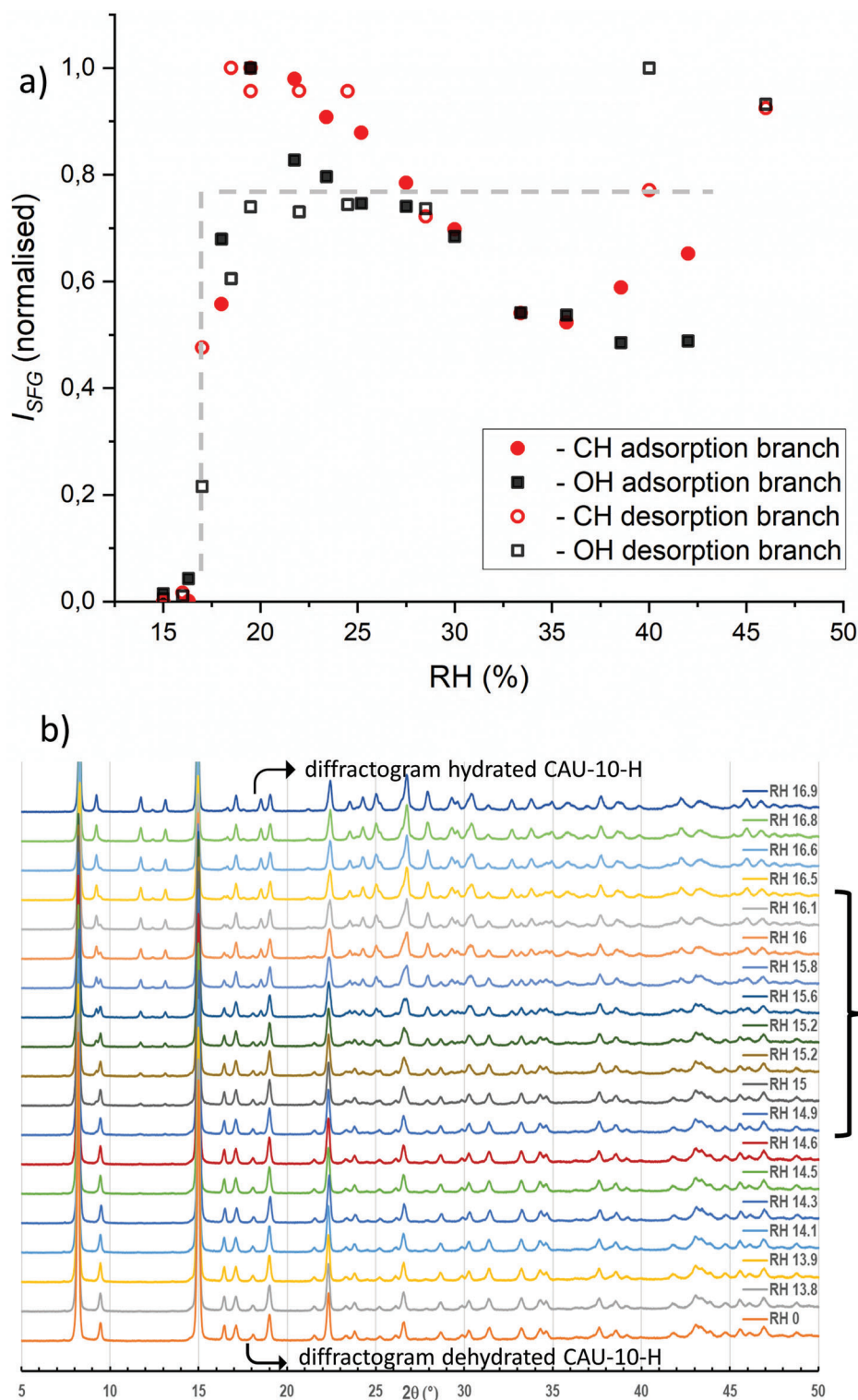
Figure 3. Activated CAU-10-H. a) Normalized SFG intensity of v(–OH) (black squares) and v(–CH) (red circles) stretching peaks as a function of decreasing (empty symbols) and increasing (filled symbols) relative humidity values. Gray dashed line: guide-to-the-eye to indicate the trend found in all datasets, ignoring the variations due to OPA instability that are unique to each measurement. b) PXRD patterns as a function of relative humidity, measured at 40 °C. The chronology of the experiments was from low to high humidity (from bottom to top).
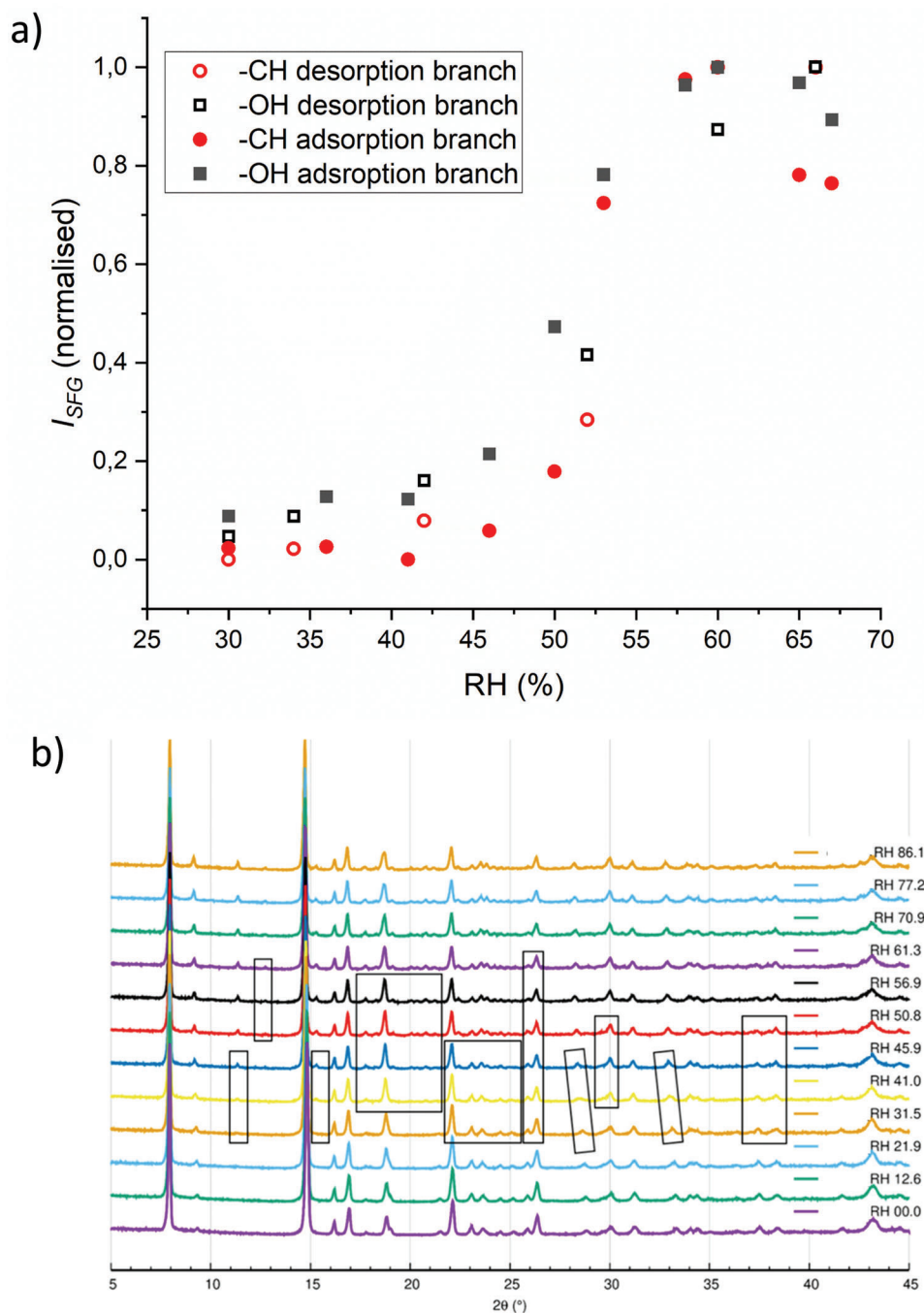
Figure 4. Characterization of activated CAU-10-CH$_3$. a) Normalized SFG intensity of ν(−OH) (black squares) and ν(−CH) (red circles) stretching peaks as a function of decreasing (empty symbols) and increasing (filled symbols) relative humidity values. b) PXRD patterns as a function of relative humidity, measured at 40 °C. The areas of the diffractogram that strongly change with increasing relative humidity are depicted by the rectangular boxes as guides-to-the-eye.

of the pentamer (O1 and O1^1) can form much weaker hydrogen bonds with framework carboxylate oxygen atoms (O1...O$_f$3 distance of 3.73 Å). This may explain the observation that for the double pentamer, including the four tethering water molecules (O5) at the base, the oxygen atoms have full occupancy, meaning the water is present at this site in all unit cells. In contrast, the positions of the water molecules at the top of the pentamers (O3)

are only partially occupied (0.3 occupancy) (Figure S2.2.1, Supporting Information). All O⋯O distances of neighboring water molecules within the cluster are within 2.8–3 Å, indicating favorable hydrogen bonding configurations.

A (H$_2$O)$_{14}$-cluster—which contains all water molecules with full occupancy in the single crystal XRD refined structure—per pore corresponds to 0.32 g g^{-1} adsorbed water, exactly the
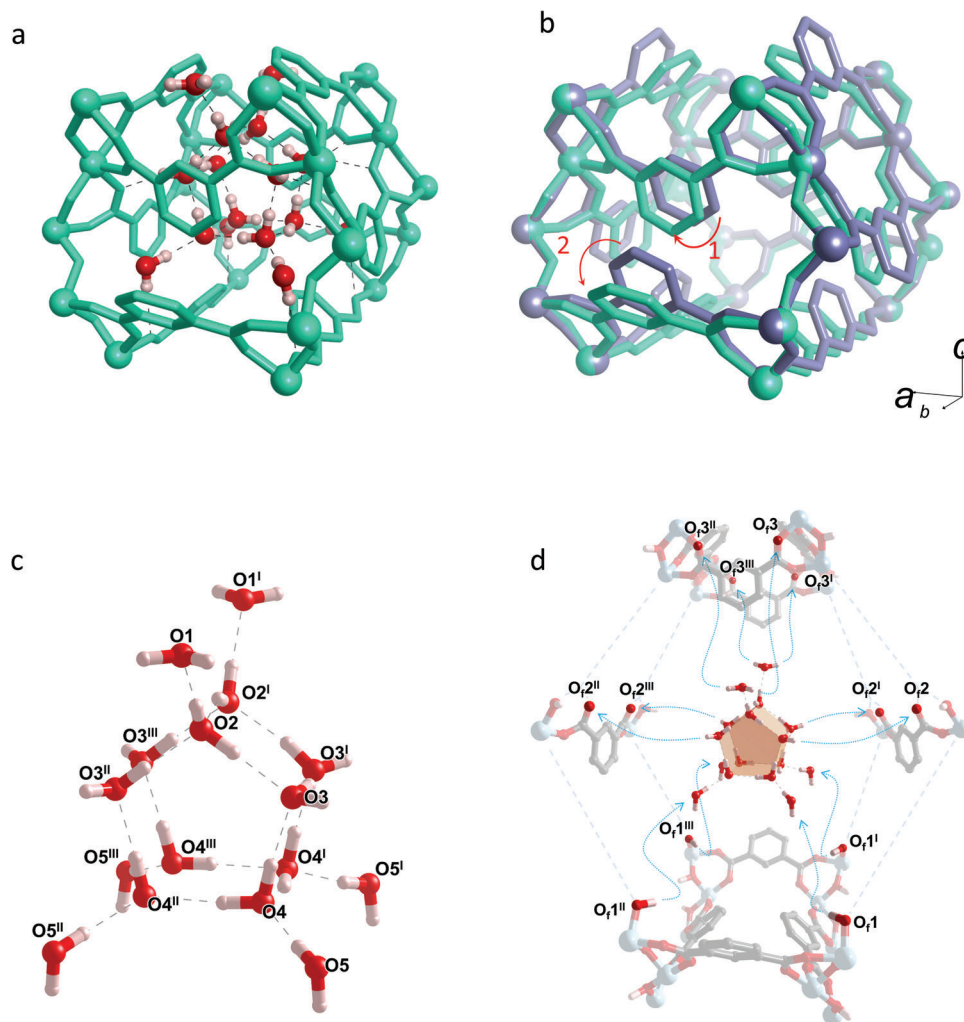
2210050 (6 of 13)

**ADVANCED
SCIENCE NEWS**

www.advancedsciencenews.com

**ADVANCED
MATERIALS**

www.advmat.de

Figure 5. a) $(H_2O)_{16}$ water cluster in hydrated CAU-10-H cavity, b) comparison between the hydrated non-centrosymmetric CAU-10-H (green) and centrosymmetric dehydrated CAU-10-H (blue) structure, water molecules omitted, c) $(H_2O)_{16}$ water cluster found in hydrated CAU-10-H with labeled oxygen atoms, and d) expanded hydrated CAU-10-H cavity with $(H_2O)_{16}$ water cluster, explicitly showing potential hydrogen bonds between framework and adsorbate (blue arrows). The hydrated CAU-10-H framework with contained water cluster is based on results from single-crystal XRD.

volume of adsorbed water directly after the step in the adsorption isotherm (Figure 1). The $(H_2O)_{16}$-cluster per pore corresponds to the maximum amount of adsorbed water, namely 0.37 g g^{-1} (see Figure 1). Adjacent water clusters along the pore direction do not lie within H-bonding distance. The phase transition here entails a conformational change of the isophthalate linkers containing the O_f2 atoms, as shown schematically via the red arrows in Figure 5b (Figure S2.2.5, Supporting Information). Before the phase transition, both types of isophthalate ions are symmetry-equivalent (structure previously reported based on Rietveld refinement)[29] having the same intermediate angle with the pore direction. After the phase transition, one type of isophthalate linker (indicated by arrow "1" in Figure 5b) maximizes pore space to accommodate the $(H_2O)_{14}$-cluster. The other type of isophthalate linker, indicated by the red arrow "2" in Figure 5b, protrudes further into the channel. Previously, computational results also indicated such a conformational change, as indicated by the red arrow "2" in Figure 5b, to be likely, where only after the phase

transition to the "wet" phase, the μ–OH sites become accessible for hydrogen bonding with adsorbed water.[35] Our results also indicate in the "wet" phase a reorientation of the μ–OH groups (containing the O_f1 atoms) into an overall polar alignment along the framework c-axis. This enables favorable hydrogen bonding with the water cluster. In correspondence with the SFG results, the water cluster itself also has a non-centrosymmetric geometry. Recently Hanikelet al.[26] introduced terminology to describe the water adsorption behavior for MOFs with both hydrophilic and hydrophobic components, and some interesting step behavior in the water adsorption isotherm, based on their study of MOF-303. Here water adsorption is described by initial adsorption on the hydrophilic sites (seeding stage), formation of water clusters in the hydrophobic cavities hydrogen bonded with the initially adsorbed water molecules (clustering stage, associated with the largest step in the isotherm), followed by adsorption of additional water molecules that complete a hydrogen-bonded network between the clusters (networking stage). For CAU-10-H, as

2210050 (7 of 13)

**ADVANCED
SCIENCE NEWS**

www.advancedsciencenews.com

**ADVANCED
MATERIALS**

www.advmat.de

Table 1. O••O distances for water inside CAU-10-H likely to partake in hydrogen bonding based on structure refined from single crystal XRD. Labeling of the oxygen atoms conforms to Figure 5.

| H-donor to acceptor contact	Refined distance [Å]
(within the water cluster)	
O5...O4	2.920(9)
O3...O4	2.804(9)
O2...O3	2.79(1)
O1...O2	3.03(3)
O2...O2^I	2.99(3)
O3...O3^I	2.75(2)
O4...O4^I	3.05(1)
(with the MOF framework)	
O$_f$1...O5	2.818(8)
O3...O$_f$2	3.07(1)
O1...O$_f$3	3.72(2)

Figure 6. Illustration of the water cluster formed in CAU-10-CH$_3$ issued from our DFT-optimized geometry on the fully water-saturated MOF.

indicated by the zero water content before the step in the water adsorption isotherm, the seeding and clustering stages coincide. While additional water molecules are still adsorbed after this step, they actually only form H-bonds with one cluster, sterically hindered by protruding isophthalate linkers from completing an H-bonded network.

As the growth of sufficiently large single crystals of CAU-10-CH$_3$ for single crystal XRD proved unfeasible, we have modeled the preferential structures of water inside the pores corresponding to the maximum water adsorption capacity of 0.175 g g^{-1}, corresponding to 8.75 water molecules/pore on average, this corresponds to 85% of the saturation water adsorption capacity, and is higher than the water adsorption at the end of the step in the water adsorption isotherm centered at 0.45 p/p_0 (see Figure 1). To this end, we leveraged Monte Carlo (MC) simulations and subsequent density-functional theory (DFT)-based geometry optimization. In doing so, unit cell parameters of the MOF framework were adjusted with those obtained by indexing the XRD data of the fully hydrated CAU-10-CH$_3$. Among the several MC snapshots that have been used as the starting geometry for further DFT optimization, a water-loaded structure was proposed based on the greater similarity of the simulated PXRD pattern with the experimental counterpart, as shown in Figure S6.1 in the Supporting Information. A crystallographic information file (cif) of this hydrated CAU-10-CH$_3$ structure is provided in the Supporting Information.

Like for CAU-10-H, the predicted water-loaded structure of CAU-10-CH$_3$ (**Figure 6**) also contains four water molecules that tether to the framework μ−OH groups via hydrogen bonds, as well as a cluster of 6 water molecules hydrogen bonded between each other and to the framework O$_f$2 atoms (as defined in Figure 4c). The four water molecules bonded to the μ−OH groups are not positioned such that they can make an H-bond with any other H$_2$O molecule. The main difference with the water cluster in CAU-10-H is that the square base of the double pentagon is essentially missing. The reason is that the −CH$_3$ groups protrude to prevent the water molecules from being positioned in this region. Sterically, the (H$_2$O)$_{14}$ cluster is not feasible in
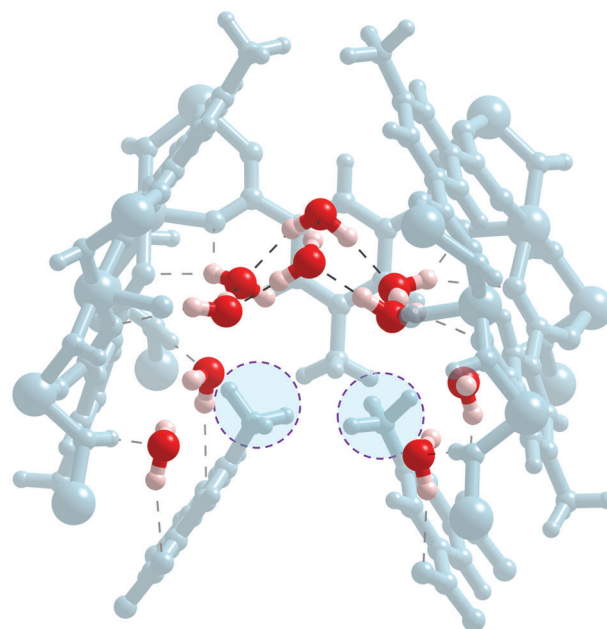
CAU-10-CH$_3$, in line with the observation that at full capacity of 0.19 g g^{-1} only 9.5 water molecules are adsorbed per pore.

The first water molecules are expected to adsorb on the μ−OH groups, in line with the humidity-dependent SFG results. The water adsorption isotherm (Figure 1) indicates that at RH% values up to 45, the water uptake is very low; then, there is a rapid increase in water uptake from 2.5 to 5.5 water molecules per pore on average (or from 0.05 to 0.11 g g^{-1}). This step behavior in water adsorption isotherms is typically due to the formation of energetically favorable water clusters due to hydrogen bonding between the water molecules (vide infra), which will be further discussed in the text based on grand canonical Monte Carlo (GCMC) simulations CAU-10-CH$_3$ at varying relative humidity.

We used DFT calculations to assess the relative affinity of the water molecules toward the CAU-10-H and CAU-10-CH$_3$ frameworks. For this purpose, we have calculated the energy difference (ΔE) between the fully optimized water-loaded structure with that of the dry phases of the respective frameworks and corresponding free water molecules. We found that the energy gain upon complete water adsorption in the CAU-10-H ($\Delta E = -1.82$ kcal (mol MOF atom)$^{-1}$) is much higher than the energy gain for the CAU-10-CH$_3$ system ($\Delta E = -0.60$ kcal (mol MOF atom)$^{-1}$).

If we make the comparison for the (H$_2$O)$_{14}$ cluster (excluding the partially occupied O1 water molecules) in CAU-10-H with free neutral water clusters, it has been found computationally that for (H$_2$O)$_{14}$ clusters, a double pentagon with a square prismatic base is the configuration with the lowest or one of the lowest energy structures.[36–38] The energy difference per water molecule for H$_2$O within this cluster with respect to free water is ≈ -10 kcal mol^{-1}.[38] The only difference is that in CAU-10-H in the bottom square, the H$_2$O molecules are further apart from each other to form hydrogen bonds with the framework μ−OH groups rather than amongst themselves. In CAU-10-H, the water

2210050 (8 of 13)

**ADVANCED
SCIENCE NEWS**

www.advancedsciencenews.com

**ADVANCED
MATERIALS**

www.advmat.de

molecules in the $(H_2O)_{14}$ cluster are on average coordinated with three other water molecules and/or μ–OH groups. In addition, four hydrogen bonds with framework O_f2 atoms can be formed. In comparison, the average coordination number of the reported energetically favorable free $(H_2O)_{14}$ cluster is 3.3. Hence, it is indeed to be expected that the formed $(H_2O)_{14}$ cluster is energetically favorable, in line with the DFT-derived MOF-water affinity. In contrast, for the $(H_2O)_6$ cluster in the hydrophobic pore of CAU-10-CH$_3$, the average coordination number is 2.3, while the four other water molecules only form a single hydrogen bond with a μ–OH. In addition, four hydrogen bonds with framework O_f2 atoms can be formed resulting in less favorable energetics of the water cluster in CAU-10-CH$_3$ versus CAU-10-H which causes the shift of the steep increase in the water adsorption isotherm to higher p/p_0 (see Figure 1).

Further grand canonical Monte Carlo (GCMC) simulations CAU-10-CH$_3$ at varying water vapor pressure showed that the first water molecules preferentially adsorb at the μ–OH sites once their accessibility is made possible by the gradual increase of the water vapor pressure, in line with the humidity-dependent SFG results (see GCMC adsorption snapshots in the Supporting Information). The experimental and simulated water adsorption isotherms (Figure 1; Figure S6.2, Supporting Information) indicate that at RH% values up to 45, water uptakes are rather low. Our GCMC calculation predicts a gradual pore filling, while a steep increase of the water uptake from 2.5 to 5.5 water molecules per pore on average (or from 0.05 to 0.11 g g^{-1}) is observed experimentally. This step behavior in water adsorption isotherms is due to the formation of energetically favorable water clusters due to hydrogen bonding between the water molecules. The resultant $(H_2O)_{5-6}$ cluster in the hydrophobic pore, as shown in Figure 6, can be bridged by additional water molecules adsorbed at the μ–OH sites (see GCMC adsorption snapshots in the ESI). This simulated behavior would be exhausted by considering the water-triggered dynamics of the –CH$_3$ groups. Indeed, we expect that when gradually more water molecules adsorb, the pore becomes more open via conformational change of the isophthalate ions into the non-centrosymmetrical arrangement shown in Figure 6. This conformational change of the isophthalate ions upon hydration is similar to that of hydrated CAU-10-H shown in Figure 5b. This is in line with the observation that the SFG signal related to the –CH vibrations becomes only significant at higher relative humidity compared to the signal related to μ–OH. However, since this GCMC simulation was performed on a static model of the dry phase of the solid, above the RH% 45, as expected, our predicted water adsorption isotherms show quite lower uptakes compared to the experimental counterpart.

These results indicate that in order to achieve a water adsorption isotherm with steep uptake, adsorption has to proceed via water cluster formation, rather than gradual adsorption of water over hydrophilic sites. Yet, the material cannot be too hydrophobic, then steep adsorption via cluster formation also occurs, albeit at too high p/p_0.[3–5] The sites of medium hydrophilicity of CAU-10-H, namely μ–OH, seem to fulfill the role of shifting the step to lower p/p_0, while most of the framework still consists of hydrophobic pore walls. The geometry of the cavity allows for an energetically favorable water cluster (average number of H-bonds per water of 3.3). These factors together allow for steep water adsorption within the desired p/p_0 range. In CAU-10-CH$_3$, one

of these elements is missing: the –CH$_3$ groups sterically hinder the formation of an energetically favorable water cluster (average number of H-bonds per water of 2.2), the result being that the desired water adsorption behavior is not observed. To summarize, these results suggest that to achieve a water adsorption isotherm with steep uptake in the area of technological interest, a MOF should consist of: i) hydrophobic cavities with a geometry that can accommodate an energetically favorable water cluster and ii) a few sites of medium hydrophilicity. To validate this hypothesis, we investigated a database of water adsorption isotherms of MOFs taken from the archive of water adsorption isotherm data from the co-authors' research groups. The included water adsorption isotherms all have a significant increase in water adsorption in the 0.1–0.3 p/p_0 range, and/or a steep step somewhere in the water adsorption isotherm. We gathered 28 datasets of 16 different MOFs, all microporous except MIL-100(Cr). As an inverse measure for the steepness, we took the difference between the relative pressure at 75% and at 25% of the total capacity: $\Delta p/p_0^{(75\%-25\%)}$. The Henry constant, a measure for the affinity of the adsorbent for water at the lowest loadings (defined in Section 7, Supporting Information) versus $\Delta p/p_0^{75\%-25\%}$ is plotted in **Figure 7**a. In Figure 7b, the Henry constant of different MOFs is plotted versus the relative pressure at half capacity α. In Figure S7.1 (Supporting Information), the Henry constant, the relative pressure at half capacity α and $\Delta p/p_0^{(75\%-25\%)}$ are plotted versus total water adsorption capacity. No correlation between these quantities and the total water adsorption capacity can be observed. In Figure S7.2 (Supporting Information), graphs equivalent to those in Figure 6 can be found, with the added information on the temperature at which the water adsorption isotherms (from 288 K to 313 K) were measured. As can be seen from the data where the same MOF was measured at different temperatures (CAU-10-H, KMF-1, and NH$_2$-MIL-125), temperature has only a limited effect on the values of the different quantities.

A high value of $\Delta p/p_0^{(75\%-25\%)}$ means the adsorption is progressive and continuous, while a low value implies the sudden uptake of large quantities of water. In Figure 7a, we do see a clear correlation between the Henry constant and $\Delta p/p_0$, where water uptake becomes more gradual as the Henry constant increases, which means that the material has more hydrophilic sites. This is in line with previous observations that linkers functionalized with –OH and –NH$_2$, hence hydrophilic sites, decrease the slope of the adsorption isotherm at intermediate loadings.[34,35] An example is NH$_2$-UiO-66 compared to UiO-67. UiO-67 shows a single steep at 0.55 p/p_0, adding the hydrophilic –NH$_2$ groups leads to a large, though more gradual increase centered at 0.22 p/p_0, albeit with a smaller slope and also significant water uptake at low p/p_0.[40] Also, MOFs with coordinatively unsaturated sites, which are very hydrophilic, have a high Henry constant and often gradual water adsorption. Examples are MIL-100(Cr) (Figure 6), CPO-27(Ni),[41] HKUST-1,[23] MIL-100(Fe)[23] and Y-shp-MOF-5.[11] From these data, it seems that the Henry constant needs to be low to achieve a steep uptake curve. This is in line with our hypothesis that for steep water adsorption isotherms, the material has to be hydrophobic. The water adsorption slope approaching infinity is an extreme example of a type-V isotherm, where adsorbate-adsorbate interactions are stronger than adsorbate-adsorbent ones. A sudden uptake of a large amount of water molecules is thus indicative of adsorption
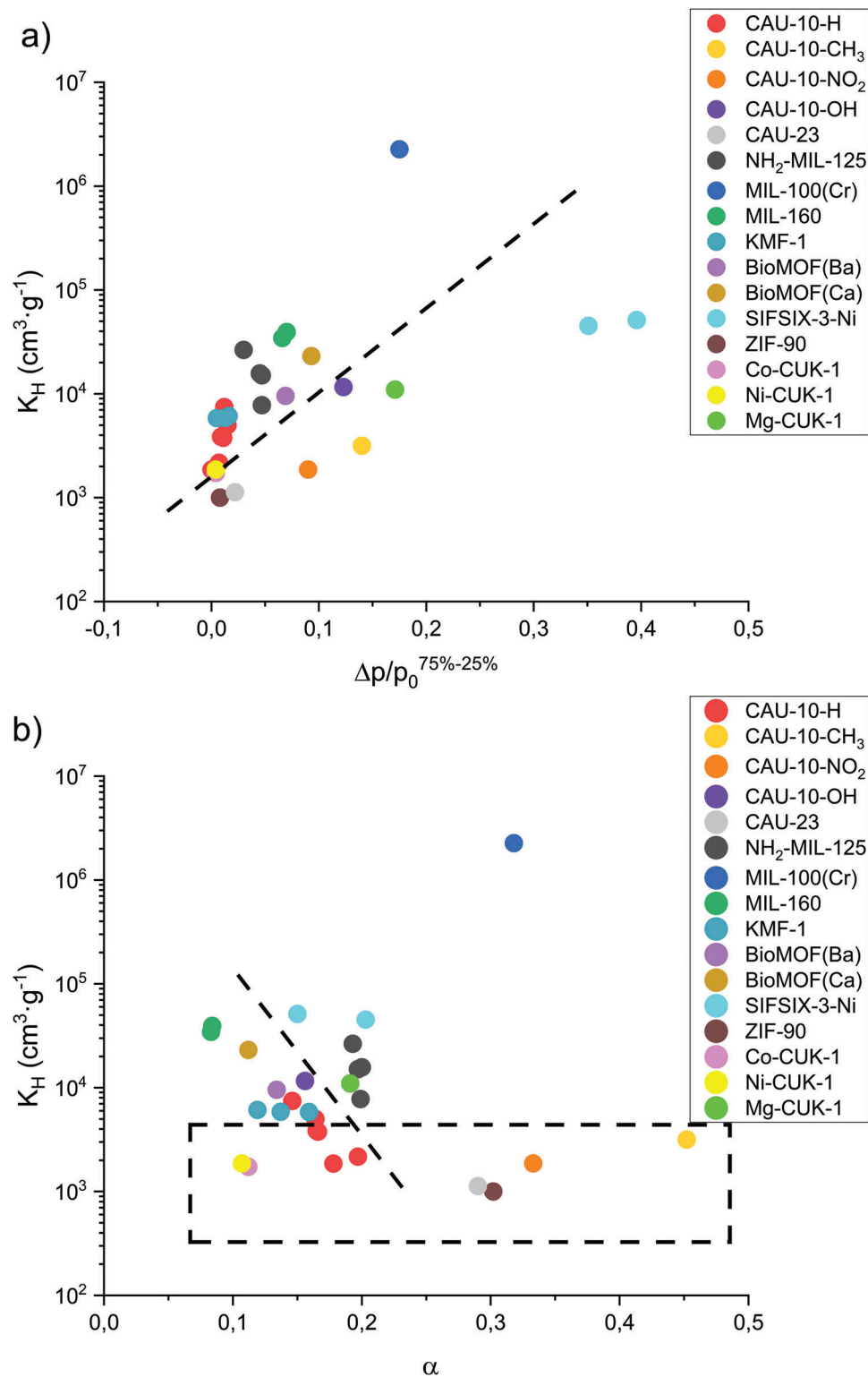
Figure 7. a,b) The Henry constant K_H of the 24 datasets plotted versus the difference between the relative pressure at 75% and 25% of the total capacity $\Delta p/p_0^{(75\%-25\%)}$ (a) and the relative pressure at half capacity α (b). The lines are guides-to-the-eye. The box in (b) highlights the materials with low K_H. In part data are published in refs. [27–29,42,44,48–50] and in part data made available in a data repository (see Acknowledgements and Data Availability Statement).

ADVANCED
SCIENCE NEWS

www.advancedsciencenews.com

ADVANCED
MATERIALS

www.advmat.de

occurring through favorable water cluster formation. This is corroborated by the fact that for several MOFs that show a very steep water uptake, specific positions for the oxygen atoms of occluded water molecules have been found, e.g., for MOF-801(Zr)[24] and CUK-1(Co/Ni/Mg).[28] The materials in Figure 7a, that show a slope approaching infinity are ZIF-90, CAU-10-H, CAU-23,[28] KMF-1[5,42] and Co- and Ni-CUK-1. These frameworks all have a few sites that can partake in hydrogen bonds, but that are of medium hydrophilicity, containing μ–OH, aldehyde groups, and aromatic sulfur and oxygen, next to aromatic hydrophobic pore walls, in line with our hypothesis.

In Figure 7b, the Henry constant of the 16 different MOs is plotted versus the relative pressure at half capacity α. Canivet et al.[39] reported previously for a sample of 15 MOFs that contained α-values from 0,02 to 0,95, a modest correlation in which α decreases as the Henry constant increases. Our selection of materials contains mainly α-values in the range of technological interest (0.1–0.3 p/p_0). Also, we find the same modest correlation: α decreases as the Henry constant increases. This is in line with the expectation that a more hydrophilic material (high k_H) adsorbs water at lower relative humidity values. The outlier here is MIL-100(Cr). This is the only mesoporous material in the selection, which makes it mechanistically outside of the scope of this paper which aims to understand water adsorption behavior in microporous MOFs.

If we consider specifically the materials that show a very steep water adsorption isotherm, hence having a very low Henry constant of $\approx 10^3$ cm^3 g^{-1} (see Figure 7a), we see a very large variation of the α-value between 0.1 and 0.45 p/p^F (see Figure 7b). This indicates that for these hydrophobic materials, the energetics of the formed water clusters are quite different: the more favorable cluster formation is energetic, the lower the α-value will be. This is also in line with our hypothesis that the geometry of the hydrophobic cavity determines how energetically favorably a water cluster can be formed, and hence the value of α. α is low for cavities that allow for very favorable water clusters (e.g., CAU-10-H) and high for cavities that do not allow for such clusters (e.g., CAU-10-CH$_3$). Other MOFs outside this work that show very steep water uptake are MOF-801(Zr) ($\alpha \approx 0.1$),[24] Al-fumarate ($\alpha \approx 0.22$),[25] MOF-841(Zr)($\alpha \approx 0.25$),[24] UiO-67 ($\alpha \approx 0.55$),[40] MIL-68(In)[39] ($\alpha \approx 0.58$), and NH$_2$-MIL-68[39] ($\alpha \approx 0.42$). They also contain the features that we here identify as necessary for this behavior: hydrophobic pore walls (aromatic or alkene ligands) and framework μ–OH groups, and there is even an example containing NH$_2$ groups. Their α-value varies between 0.1 and almost 0.6, indicating very different energetics of the formed water clusters. The importance of pore geometry cannot be reduced to, e.g., simply pore diameter, in line with the previous results of Furukawa et al.[24] Yet, the examples showing a very high α, UiO-67 and (NH$_2$-)MIL-68, all contain supermicropores. This is in line with the observation that activated carbons with similar O/C ratios, α shift to higher values as the pore size increases, due to the fact that the larger water clusters needed for pore filling require a larger chemical potential.[3]

To understand the limits of our hypothesis, we searched the literature for counterexamples that show steep water uptake in the area of technological interest, but that do not have our hypothesized structure of hydrophobic cavity plus sites of medium hydrophilicity and discuss them here. While MOFs with coordinatively unsaturated sites, which are very hydrophilic, generally show gradual uptake of water, a few examples can be found, where initial adsorption on an unsaturated site at the start of the water isotherm, is followed by a steep step change in the water adsorption isotherm at higher relative humidity. Part of the adsorption capacity will be lost by the water adsorbed at $p/p_0 < 0.1$. One of these exceptions is a porous coordination polymer based on Cu^{2+} and isophthalate ions reported by Ichii et al.[43] The framework is structured such that after adsorption of water on unsaturated Cu^{2+} sites at very low relative humidity, a very steep water adsorption step occurs at 4 RH% in which water is absorbed as cubane clusters each tethered via hydrogen bonds to four water molecules residing on open metal sites. These cubane clusters are exactly commensurate with the framework, explaining the steep water adsorption isotherm. Similarly, for Fe-MIL-59, hydrophilic water uptake at very low relative humidity is followed by a step at ≈ 0.13 p/p_0, which corresponds to filling of the hydrophobic pores with clusters for which specific positions of the oxygen atoms of the water molecules were found, and where these water molecules are tethered via hydrogen bonds to water molecules in the hydrophilic pores.[44] A unique example is a mesoporous MOF with 1-D pores and Co^{2+} open metal sites (Co$_2$Cl$_2$(BTDD)) with BTDD = bis(1H-1,2,3-triazolo[4,5-b],[4′,5′-i])dibenzo[1,4]dioxin). The specific mechanism is related to water filling of mesopores with a diameter just below the critical diameter for capillary condensation. As this is a mechanism specific to mesoporous materials, it will not be further discussed here.[45,46] In the alternative cases, it seems that the water adsorbed at very hydrophilic sites (e.g., H$_2$O at unsaturated metal sites) can also function as the site of intermediate hydrophilicity on which cluster formation in an otherwise hydrophobic framework can take place, essentially the favorable adsorption mechanism outlined in this paper. That only very few examples can be found suggests that obtaining the right energetics of the water cluster in the latter examples could be more delicate. As a last note, many metal–organic frameworks show complex multistep water adsorption behavior by virtue of having different types of pores. An illustrative example is DUT-67.[47] There is a first smaller step below 0.1 p/p_0 corresponding to small, hydrophilic cavities. The largest and steepest steps occur at 0.3 and 0.35 p/p_0. Each of these two steps corresponds to rather hydrophobic aromatic cavities, which contain some μ–O sites of medium hydrophilicity. The difference between the two cavities is that in the one that adsorbs water at lower relative humidity, the water molecules can interact with the sulfur atoms of the thiophene-containing organic linkers, while in the more hydrophobic cage, they cannot. Both these steps in this multistep adsorption isotherm can thus still be described via the model proposed in this paper.

3. Conclusion

We found that CAU-10-X (X = H, CH$_3$, NO$_2$, OH) all undergo a centro- to non-centrosymmetric phase transition upon water adsorption, as demonstrated by SFG and SHG. For CAU-10-H and CAU-10-CH$_3$, frameworks with the same topology and similar balance between hydrophobic and hydrophilic components, the origin of their vastly different water adsorption properties are assigned to the formation of an energetically far more favorable water cluster in CAU-10-H versus CAU-10-CH$_3$. For CAU-10-H,

ADVANCED
SCIENCE NEWS

www.advancedsciencenews.com

ADVANCED
MATERIALS

www.advmat.de

an energetically favorable 14 water cluster is identified, which fits in the hydrophobic pore and is tethered via hydrogen bonds to four framework Al–OH groups. The high amount of hydrogen bonding within the cluster (3.28 H-bonds per water molecule) cause favorable energetics leading to the abrupt formation of the entire water cluster at a specific relative humidity. Indeed, computationally we found that the energy gain upon complete water adsorption in the CAU-10-H ≈ -1.82 kcal (mol MOF atom)$^{-1}$. In contrast, for CAU-10-CH$_3$, the four water molecules hydrogen bonded to the μ–OH groups are isolated because of steric hindrance by two –CH$_3$ groups from the remainder of the water cluster: computationally, we found a far less energetically favorable 6-water cluster (2.3 H-bonds per water molecule). This explains the far more gradual water uptake.

In situ XRD and sum-frequency generation spectra at different relative humidity values showed a first-order phase transition accompanying water adsorption in CAU-10-H, while for CAU-10-CH$_3$, this is a higher-order phase transition. In situ sum frequency generation indicates that, most likely, the gradual water uptake started with water adsorption at the μ–OH groups and that as more water molecules adsorb, the pore is enlarged via a conformational change of the isophthalate ions, in a similar way to that of CAU-10-H upon hydration.

We found for a database of MOFs with some favorable water adsorption characteristics, that the Henry constant K_H and pressure at half the saturation capacity α are only modestly correlated. Yet we observed a low Henry constant, which means a lack of strongly hydrophilic sites, strongly correlates with sudden water uptake. This means adsorption occurs through cluster formation: $H_2O\bullet\bullet\bullet H_2O$ interactions are much stronger than framework$\bullet\bullet\bullet H_2O$ interactions. However, the pressure at half the saturation capacity α can vary vastly for materials with a low Henry constant K_H. This means that the energetics of these water clusters can differ greatly: both a favorable geometry of the pore cavities, as well as well-positioned sites of medium hydrophilicity are needed for α to be in the relative humidity window of interest.

[CCDC 2142131] contains the supplementary crystallographic data for this paper. These data can be obtained free of charge from The Cambridge Crystallographic Data Centre via www.ccdc.cam.ac.uk/data_request/cif.]

Supporting Information

Supporting Information is available from the Wiley Online Library or from the author.

Conflict of Interest

The authors declare no conflict of interest.

Data Availability Statement

The single-crystal X-ray diffraction data of hydrated CAU-10-H can be assessed and used by others for further studies at 4TU.ResearchData: https://doi-org.tudelft.idm.oclc.org/10.4121/21953906. The previously unpublished water adsorption isotherm data can be assessed and used by others for further studies at 4TR.ResearchData: https://doi-org.tudelft.idm.oclc.org/10.4121/22009211. The other data that support the findings of this study are available from the corresponding author upon reasonable request.

Keywords

[1] Y. I. Aristov, *Appl. Therm. Eng.* **2013**, *50*, 1610.

[2] H. Reinsch, B. Marszałek, J. Wack, J. Senker, B. Gil, N. Stock, *Chem. Commun.* **2012**, *48*, 9486.

[3] L. Liu, S. Tan, T. Horikawa, D. D. Do, D. Nicholson, J. Liu, *Adv. Colloid Interface Sci.* **2017**, *250*, 64.

[4] T. Kimura, H. Kanoh, T. Kanda, T. Ohkubo, Y. Hattori, Y. Higaonna, R. Denoyel, K. Kaneko, *J. Phys. Chem. B* **2004**, *108*, 14043.

[5] T. Ohba, H. Kanoh, K. Kaneko, *Chemistry* **2005**, *11*, 4890.

[6] Y. G. Bushuev, G. Sastre, J. V. De Julia, J. Ga, *J. Phys. Chem. C* **2012**, *116*, 24916.

[7] P. Ghosh, K. C. Kim, R. Q. Snurr, *J. Phys. Chem. C* **2014**, *118*, 1102.

[8] J. Canivet, A. Fateeva, Y. Guo, B. Coasne, D. Farrusseng, *Chem. Soc. Rev.* **2014**, *43*, 5594.

[9] M. F. De Lange, K. J. F. M. Verouden, T. J. H. Vlugt, J. Gascon, F. Kapteijn, *Chem. Rev.* **2015**, *115*, 12205.

[10] X. Liu, X. Wang, F. Kapteijn, *Chem. Rev.* **2020**, *120*, 8303.

[11] M. J. Kalmutzki, C. S. Diercks, O. M. Yaghi, *Adv. Mater.* **2018**, *30*, 1704304.

[12] H. Kim, S. Yang, S. R. Rao, S. Narayanan, E. A. Kapustin, H. Furukawa, A. S. Umans, O. M. Yaghi, E. N. Wang, *Science* **2017**, *356*, 430.

[13] N. Hanikel, M. S. Prévot, F. Fathieh, E. A. Kapustin, H. Lyu, H. Wang, N. J. Diercks, T. G. Glover, O. M. Yaghi, *ACS Cent. Sci.* **2019**, *5*, 1699.

[14] H. A. Almassad, R. I. Abaza, L. Siwwan, B. Al-Maythalony, K. E. Cordova, *Nat. Commun.* **2022**, *13*, 4873.

[15] H. Kakiuchi, S. Shimooka, M. Iwade, K. Oshima, M. Yamazaki, S. Terada, H. Watanabe, T. Takewaki, *Kagaku Kogaku Ronbunshu* **2005**, *31*, 361.

[16] N. Floquet, J. P. Coulomb, N. Dufau, G. Andre, *J. Phys. Chem. B* **2004**, *108*, 13107.

[17] L. B. McCusker, Ch. Baerlocher, E. Jahn, M. Bülow, E. Jahn, *Zeolites* **1991**, *11*, 308.

[18] M. E. Davis, C. Montes, P. E. Hathaway, J. P. Arhancet, D. L. Hasha, J. M. Garces, *J. Am. Chem. Soc.* **1989**, *111*, 3919.

**ADVANCED
SCIENCE NEWS**

www.advancedsciencenews.com

**ADVANCED
MATERIALS**

www.advmat.de

[19] S. M. T. Abtab, D. M. Alezi, P. Bhatt, A. Shkurenko, Y. Belmabkhout, H. Aggarwal, Ł. J. Weseliński, N. Alsadun, U. Samin, M. N. Hedhili, M. Eddaoudi, *Chem* **2018**, *4*, 94.

[20] Z. Chen, P. Li, X. Zhang, P. Li, M. C. Wasson, T. Islamoglu, J. F. Stoddart, O. K. Farha, *J. Am. Chem. Soc.* **2019**, *141*, 2900.

[21] P. M. Schoenecker, C. G. Carson, H. Jasuja, C. J. J. Flemming, K. S. Walton, *Ind. Eng. Chem. Res.* **2012**, *51*, 6513.

[22] B. Coasne, A. Galarneau, R. J. M. Pellenq, F. Di Renzo, *Chem. Soc. Rev.* **2013**, *42*, 4141.

[23] P. Küsgens, M. Rose, I. Senkovska, H. Fröde, A. Henschel, S. Siegle, S. Kaskel, *Microporous Mesoporous Mater.* **2009**, *120*, 325.

[24] H. Furukawa, F. Gándara, Y. B. Zhang, J. Jiang, W. L. Queen, M. R. Hudson, O. M. Yaghi, *J. Am. Chem. Soc.* **2014**, *136*, 4369.

[25] F. Jeremias, D. Fröhlich, C. Janiak, S. K. Henninger, *RSC Adv.* **2014**, *4*, 24073.

[26] N. Hanikel, X. Pei, S. Chheda, H. Lyu, W. Jeong, J. Sauer, L. Gagliardi, O. M. Yaghi, *Science* **2021**, *374*, 454.

[27] D. Lenzen, J. Zhao, S.-J. Ernst, M. Wahiduzzaman, A. K. Inge, D. Fröhlich, H. Xu, H.-J. Bart, C. Janiak, S. Henninger, G. Maurin, X. Zou, N. Stock, *Nat. Commun.* **2019**, *10*, 3025.

[28] J. S. Lee, J. W. Yoon, P. G. M. Mileo, K. H. Cho, J. Park, K. Kim, H. Kim, M. F. De Lange, F. Kapteijn, G. Maurin, S. M. Humphrey, J. S. Chang, *ACS Appl. Mater. Interfaces* **2019**, *11*, 25778.

[29] H. Reinsch, M. A. van der Veen, B. Gil, B. Marszalek, T. Verbiest, D. E. De Vos, N. Structures Stock, *Chem. Mater.* **2013**, *25*, 17.

[30] M. v. Solovyeva, A. I. Shkatulov, L. G. Gordeeva, E. A. Fedorova, T. A. Krieger, Y. I. Aristov, *Langmuir* **2021**, *37*, 693.

[31] D. Fröhlich, E. Pantatosaki, P. D. Kolokathis, K. Markey, H. Reinsch, M. Baumgartner, M. A. van der Veen, D. E. De Vos, N. Stock, G. K. Papadopoulos, S. K. Henninger, C. Janiak, *J. Mater. Chem. A* **2016**, *4*, 11859.

[32] D. Fröhlich, S. K. Henninger, C. Janiak, *Dalton Trans.* **2014**, *43*, 15300.

[33] A. Cadiau, J. S. Lee, D. Damasceno Borges, P. Fabry, T. Devic, M. T. Wharmby, C. Martineau, D. Foucher, F. Taulelle, C. H. Jun, Y. K. Hwang, N. Stock, M. F. De Lange, F. Kapteijn, J. Gascon, G. Maurin, J. S. Chang, C. Serre, *Adv. Mater.* **2015**, *27*, 4775.

[34] S. Canossa, A. Gonzalez-Nelson, L. Shupletsov, M. del Carmen Martin, M. A. Van der Veen, *Chemistry* **2020**, *26*, 3564.

[35] I. v. Grenev, A. A. Shubin, M. v. Solovyeva, L. G. Gordeeva, *Phys. Chem. Chem. Phys.* **2021**, *23*, 21329.

[36] S. Maheshwary, N. Patel, N. Sathyamurthy, A. D. Kulkarni, S. R. Gadre, *J. Phys. Chem. A* **2001**, *105*, 10525.

[37] A. Rakshit, P. Bandyopadhyay, J. P. Heindel, S. S. Xantheas, *J. Chem. Phys.* **2019**, *151*, 214307.

[38] A. Malloum, J. J. Fifen, Z. Dhaouadi, S. G. Nana Engo, J. Conradie, *New J. Chem.* **2019**, *43*, 13020.

[39] J. Canivet, J. Bonnefoy, C. Daniel, A. Legrand, B. Coasne, D. Farrusseng, *New J. Chem.* **2014**, *38*, 3102.

[40] N. Ko, J. Hong, S. Sung, K. E. Cordova, H. J. Park, J. K. Yang, J. Kim, *Dalton Trans.* **2015**, *44*, 2047.

[41] E. Elsayed, R. Al-Dadah, S. Mahmoud, A. Elsayed, P. A. Anderson, *Appl. Therm. Eng.* **2016**, *99*, 802.

[42] K. H. Cho, D. D. Borges, U.-H. Lee, J. S. Lee, J. W. Yoon, S. J. Cho, J. Park, W. Lombardo, D. Moon, A. Sapienza, G. Maurin, J.-S. Chang, *Nat. Commun.* **2020**, *11*, 5112.

[43] T. Ichii, T. Arikawa, K. Omoto, N. Hosono, H. Sato, S. Kitagawa, K. Tanaka, *Commun. Chem.* **2020**, *3*, 16.

[44] D. Lenzen, J. G. Eggebrecht, P. G. M. Mileo, D. Fröhlich, S. Henninger, C. Atzori, F. Bonino, A. Lieb, G. Maurin, N. Stock, *Chem. Commun.* **2020**, *56*, 9628.

[45] A. J. Rieth, K. M. Hunter, F. Paesani, *Nat. Commun* **2019**, *10*, 4771.

[46] A. J. Rieth, S. Yang, E. N. Wang, M. Dincă, *ACS Cent. Sci.* **2017**, *3*, 668.

[47] V. Bon, I. Senkovska, J. D. Evans, M. Wöllner, M. Hölzel, S. Kaskel, *J. Mater. Chem. A* **2019**, *7*, 12681.

[48] M. F. De Lange, T. Zeng, T. J. H. Vlugt, J. Gascon, F. Kapteijn, *CrystEngComm* **2015**, *17*, 5911.

[49] A. Permyakova, O. Skrylnyk, E. Courbon, M. Affram, S. Wang, U. H. Lee, A. H. Valekar, F. Nouar, G. Mouchaham, T. Devic, G. De Weireld, J. S. Chang, N. Steunou, M. Frère, C. Serre, *ChemSusChem* **2017**, *10*, 1419.

[50] T. Grancha, J. Ferrando-Soria, J. Cano, P. Amorós, B. Seoane, J. Gascon, M. Bazaga-García, E. R. Losilla, A. Cabeza, D. Armentano, E. Pardo, *Chem. Mater.* **2016**, *28*, 4608.

2210050 (13 of 13)